JOURNAL OF GEOPHYSICAL RESEARCH, VOL. 90, NO. D6, PAGES 10,607–10,619, OCTOBER 20, 1985

Latitudinal Variation of Spectral Optical Thickness and Columnar Size Distribution of the El Chichon Stratospheric Aerosol Layer

JAMES D. SPINHIRNE AND MICHAEL D. KING

Laboratory for Atmospheres, NASA Goddard Space Flight Center, Greenbelt, Maryland

Multiwavelength solar radiometer observations of directly transmitted solar radiation have been obtained at 10 discrete wavelengths between 0.440 and 2.233 μm during an airborne latitudinal survey in late April and early May 1983. These observations have been used to derive the spectral optical thickness of the El Chichon stratospheric aerosol layer from 68°N to 56°S. The stratospheric optical thicknesses 1 year after the eruptions of El Chichon were still greatly enhanced over background levels for the stratosphere. The maximum optical thickness of 0.14 (0.670-μm wavelength) was found at 50°N, rather than at 20°N as was found during an airborne latitudinal survey in late October and early November 1982. Columnar aerosol size distributions have been inferred from the 1982 and 1983 data sets by numerically inverting the aerosol optical thickness measurements as a function of wavelength. In May 1983, latitudes north of 5°S had bimodal stratospheric aerosol size distributions, while latitudes south of 5°S had monomodal size distributions. During October 1982, when optical thickness measurements were obtained only from 0.440 to 0.871 μm, the size distributions showed a strong latitudinal variation but were everywhere monomodal. For both dates the northern hemisphere distribution indicated a significantly higher ratio of large particles to small particles than the southern hemisphere distribution. The addition of the near-infrared wavelengths in the May 1983 experiment increased the accuracy of the size distribution determinations at the large-particle end of the spectrum, as anticipated, but was also found to increase the accuracy at the small-particle end.

1. INTRODUCTION

The eruptions of El Chichon in Chiapas, Mexico, from March 28 to April 4, 1982, are now recognized as a major geophysical event. The mass of particulates ultimately produced from these eruptions makes El Chichon one of the two or three largest volcanos to perturb the stratosphere this century. Most significantly, the eruptions have provided a current opportunity to study the atmospheric effects of a large volcanic injection. Observational studies of the event are providing a test for models of stratospheric transport and diffusion, aerosol radiative effects on climate, and the physics and chemistry of stratospheric aerosols [*Pollack and Ackerman*, 1983; *King et al.*, 1984]. Furthermore, an extensive series of experimental studies has been undertaken to record the characteristics and history of the El Chichon aerosol layer. These studies have included both the continuation of preexisting aerosol observational programs as well as new measurement programs aimed at characterizing the aerosol from this very massive stratospheric perturbation. In situ measurements from balloons and high-altitude aircraft have provided direct observations of the composition and size distribution of the aerosol particles at specific locations [*Hofmann and Rosen*, 1983*a*, *b*, 1985; *Oberbeck et al.*, 1983]. Satellite sensors have also observed the general global location and altitude of the layer, as well as monitored its spread [*Barth et al.*, 1983].

In order to provide a more detailed picture of the global distribution of aerosol properties of the El Chichon stratospheric layer, NASA sponsored a series of experiments to study the eruption cloud from an underflying aircraft. Included in the aircraft latitudinal surveys were measurements of the vertical distribution of aerosol backscattering by lidar [*McCormick and Swissler*, 1983; *McCormick et al.*, 1984], SO_2 and O_3 concentrations [*Evans and Kerr*, 1983], and diffuse and total radiation. In addition, direct solar photometric observations of spectral aerosol optical thickness were made. Optical thickness is of basic importance for aerosol radiation effects, but also from the measurements one may derive the related aerosol size distribution. A primary objective of the photometric measurements was therefore to observe latitudinal variations of aerosol size distribution and to obtain the size distribution at latitudes where in situ measurements had not been made, most notably in the southern hemisphere.

We have reported in a previous paper [*Spinhirne*, 1983] the spectral optical thickness results from a flight survey in October and early November 1982 (hereafter referred to as the October 1982 mission). Photometric optical thickness measurements obtained during a December 1982 NASA flight have been presented by *Dutton and Deluisi* [1983*a*]. In this paper we will present additional spectral aerosol optical thickness measurements obtained during an aircraft flight of late April and early May 1983 (hereafter referred to as the May 1983 mission). The May observations included measurements at 10 discrete wavelengths from 0.440 to 2.233 μm and covered latitudes from 68°N to 56°S. Aerosol size distributions obtained by inverting the aerosol optical thickness measurements as a function of wavelength are presented. Size distribution results were also obtained for the aircraft flight of October 1982, when optical thickness measurements were acquired at six wavelengths from 0.440 to 0.871 μm over latitudes from 44°N to 36°S. The extended wavelength capability of the May 1983 experiment was developed in part to improve the accuracy and radius range sensitivity of the aerosol size distribution determinations. The results presented here represent an initial application of solar photometric observations at wavelengths beyond 2.0 μm and the first aerosol size distributions obtained by inverting optical thickness measurements which include wavelengths greater than about 1.0 μm.

2. MEASUREMENT OF OPTICAL THICKNESS

The spectral optical thickness of the stratosphere was obtained by making observations of the directly transmitted solar radiation using narrowband, multiwavelength solar radi-

Paper number 5D0459.

TABLE 1. Spectral Channels and Bandwidths for Multiwavelength Solar Radiometers

Channel	Radiometer	Central Wavelength, μm	Spectral Resolution, μm
1	visible	0.440	0.010
2	visible	0.557	0.010
3	visible	0.612	0.010
4	visible	0.670	0.010
5	visible	0.779	0.010
6	visible	0.871	0.010
1	infrared	1.031	0.010
2	infrared	1.225	0.010
3	infrared	1.550	0.010
4	infrared	2.233	0.024

ometers (i.e., sun photometers). The measurements were obtained from an aircraft platform where it was necessary to view the sun through fixed windows on the exterior of the airframe. The measurement procedure thus included a correction for transmission losses through the windows. The governing equation for the optical thickness measurements may be written as

$$V(\lambda) = V_0(\lambda) f(t) T_w(\lambda, \theta_i) \exp [-\tau_t(\lambda) m(\theta_0)] \quad (1)$$

In this expression, $V(\lambda)$ is the measured radiometer voltage at wavelength λ, $V_0(\lambda)$ is the voltage the radiometer would measure when viewing the sun at the top of the atmosphere and the mean earth-sun distance, $f(t)$ is the factor necessary to account for the eccentricity of the earth's orbit at the time of observation t, $T_w(\lambda,\theta_i)$ is the window transmission function at the solar incidence angle θ_i, $m(\theta_0)$ is the relative atmospheric air mass at aircraft altitude, a function of solar zenith angle θ_0, and $\tau_t(\lambda)$ is the total atmospheric optical depth above the aircraft. The aerosol optical depth $\tau_a(\lambda)$ is determined from the total optical depth by subtracting the molecular optical depth $\tau_m(\lambda)$ and, for wavelengths where there is appreciable gaseous absorption, the absorption optical depth $\tau_g(\lambda)$ as follows:

$$\tau_a(\lambda) = [1/m(\theta_0)] \ln [V_0(\lambda) f(t) T_w(\lambda, \theta_i)/V(\lambda)] - \tau_m(\lambda) - \tau_g(\lambda) \quad (2)$$

A critical factor for the optical thickness observations is the expected error of the result. Since many of the sources of error are likely to be systematic, rather than random, the uncertainty in the aerosol optical thickness σ_{τ_a} may be approximated by

$$\sigma_{\tau_a} = [1/m(\theta_0)](\sigma_V/V + \sigma_{V_0}/V_0 + \sigma_{T_w}/T_w + \tau_t \sigma_m) + \sigma_{\tau_g} \quad (3)$$

where σ_V, σ_{V_0}, σ_{T_w}, σ_m, and σ_{τ_g} are uncertainty estimates for V, V_0, T_w, m, and τ_g, respectively. The most significant error source in this expression is usually the calibration error σ_{V_0}, and thus the uncertainty in the aerosol optical thickness is the smallest when the air mass is large. For air mass values larger than about 6, however, small inaccuracies in timing and location coordinates, plus variations in the vertical distribution of the attenuating species, may result in a significant uncertainty in the air mass determination [*Thomason et al.*, 1982]. For air mass values less than about 6, the air mass uncertainty may largely be neglected. The air mass values used in the present investigation were obtained from the relationship given by *Uplinger* [1981].

The factors most critical to the accuracy of the airborne determination of optical thickness are the instrument calibration coefficients, the window transmission functions, and the corrections for gaseous absorption. The instrument calibrations were obtained through the Langley method, whereby ground measurements of solar transmission as a function of air mass are extrapolated to zero air mass values. The Langley method requires a high degree of stability of the optical properties of the atmosphere during measurements [*Shaw*, 1976], and therefore observations from remote high-altitude observatories provide the most accurate results. The calibration used in processing the May 1983 aircraft observations was obtained from an average of 6 days of measurements made at Mauna Loa Observatory during July 1983. Any potential drift in the instrument calibrations was examined by comparing the results from the Langley analyses obtained during July 1983 with results from similar measurements made during March 1983. Calibration drift was less than 0.5%.

The window transmission function was calculated from standard Fresnel relationships. The windows were uncoated quartz for the visible wavelength measurements and uncoated calcium fluoride for the near-infrared measurements. The spectral optical constants of the windows were known to a high degree of precision and gave accurate transmission calculations. Tests were carried out in order to determine whether or not contamination of the windows was significant. After a standard cleaning procedure had been performed, the measured window transmittances agreed well with calculated values. Furthermore, the window transmissions were checked after the majority of flight experiments. In only one instance was the window transmission affected by contamination. In that case the error was included in the measurement uncertainty estimate.

In order to obtain the aerosol optical thickness at visible wavelengths, corrections for molecular scattering and Chappuis band ozone absorption were made using the atmospheric pressure level of the aircraft and an ozone amount independently measured by a Brewer spectrophotometer on board the aircraft [*Evans and Kerr*, 1983]. For the 11-km nominal flight altitude of the May 1983 observations, any corrections of the near-infrared wavelengths for mixed gases and water vapor absorption were found to be insignificant.

Separate instruments were used to obtain measurements in the visible and near-infrared wavelength regions. Both solar radiometers are filter wheel instruments whereby spectral selection is obtained using narrowband interference filters [*Shaw*, 1983]. The spectral characteristics and bandwidths of the radiometers are listed in Table 1. The visible solar radiometer uses a temperature-controlled silicon photodiode and has fully automated solar tracking and data acquisition systems. The near-infrared solar radiometer is a manually operated instrument that uses a lead selenide (PbSe) detector thermoelectrically cooled to -10°C. A more complete description of this instrument may be found in the work of *Spinhirne et al.* [1985].

3. Aerosol Optical Thickness Results

Measurements of the spectral optical thickness of the stratospheric aerosol layer were obtained from airborne latitudinal surveys during October 1982 and May 1983. The flight paths and dates where optical thickness measurements were collected are shown in Figure 1. The October measurements were made from the NASA Electra aircraft and the May measurements from the NASA Convair 990 aircraft. Other than operational factors such as speed, the observationally important

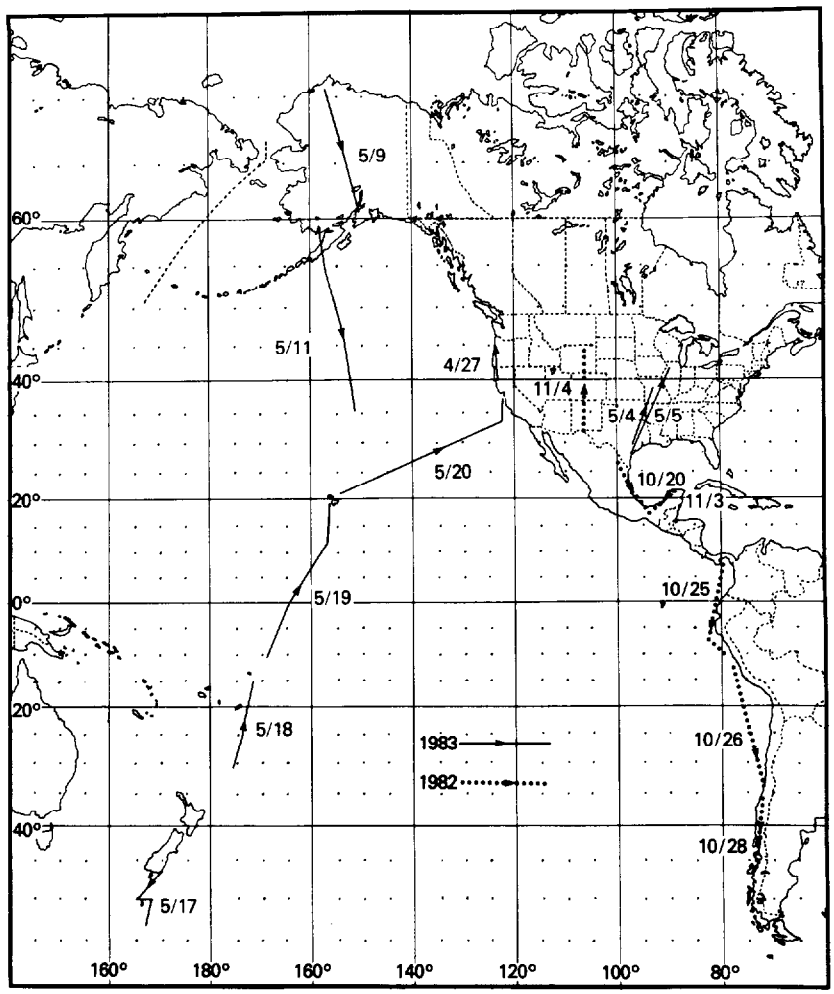

Fig. 1. Flight paths where solar radiometers collected data on the spectral optical thickness of the El Chichon stratospheric aerosol layer. Data were obtained from the NASA Electra aircraft from October 20 to November 4, 1982, and from the NASA Convair 990 aircraft from April 27 to May 20, 1983.

difference between the two aircraft was the flight altitude, which was nominally 500 mbar for the October survey and 220 mbar for the May survey. The measured aerosol optical thickness values include the component of tropospheric optical thickness which resides above the observation altitude. For the measurement from 220 mbar, the tropospheric component would not be significant. The influence of tropospheric aerosols for the 500-mbar observations have been discussed by *Spinhirne* [1983].

The spatial and temporal distribution of stratospheric optical thickness is of fundamental interest. Owing to differences in the size and composition of the particles, the optical thickness at a single wavelength does not fully describe variations in the distribution of the aerosol layer. However, the optical thickness at a given visible wavelength is a representative parameter of the particle loading and directly relates to the radiative influence of the aerosol layer. A composite of our optical thickness measurements at a wavelength of 0.670 μm is illustrated in Figure 2. A more complete measurement coverage was available for the May 1983 experiment than for the October 1982 experiment, partly as a result of the higher aircraft altitude and partly as a result of the flight plan, which was optimized for solar observations in 1983. The higher flight altitude permitted less interference from clouds during the May 1983 experiment. With the addition of the optical thicknesses derived from the 0.6943-μm monostatic lidar measurements for the October 1982 experiment, however, *Swissler et al.* [1983] were able to provide an extended latitudinal distribution for 1982.

The measured optical thicknesses were significantly enhanced over background stratospheric aerosol values at all locations where observations were obtained. The maximum value of the optical thickness at 0.670 μm was approximately 0.14 for both the October and May experiments. The region of highest optical thickness had moved from the region of 6°S–28°N in October 1982 to the region of 35°N–55°N in May 1983. Within the mid-latitude coverage of the measurements, no substantial change in the stratospheric aerosol optical thickness of the southern hemisphere was noted between the two experiments. A more complete picture of the distribution of the El Chichon eruption cloud can be obtained by considering other observations, such as the lidar airborne survey results of *McCormick et al.* [1984], optical thickness measurements from additional flights reported by *Dutton and DeLuisi* [1983*b*], and satellite observations reported by *Barth et al.* [1983].

During May 1983 a number of separate flight experiments were conducted over northern mid-latitudes at different times and locations. As is shown in Figure 2, zonal variations of the stratospheric optical thickness were evident in the observations. The zonal variation is especially evident in the region of the circumpolar front at approximately 30°N latitude. The

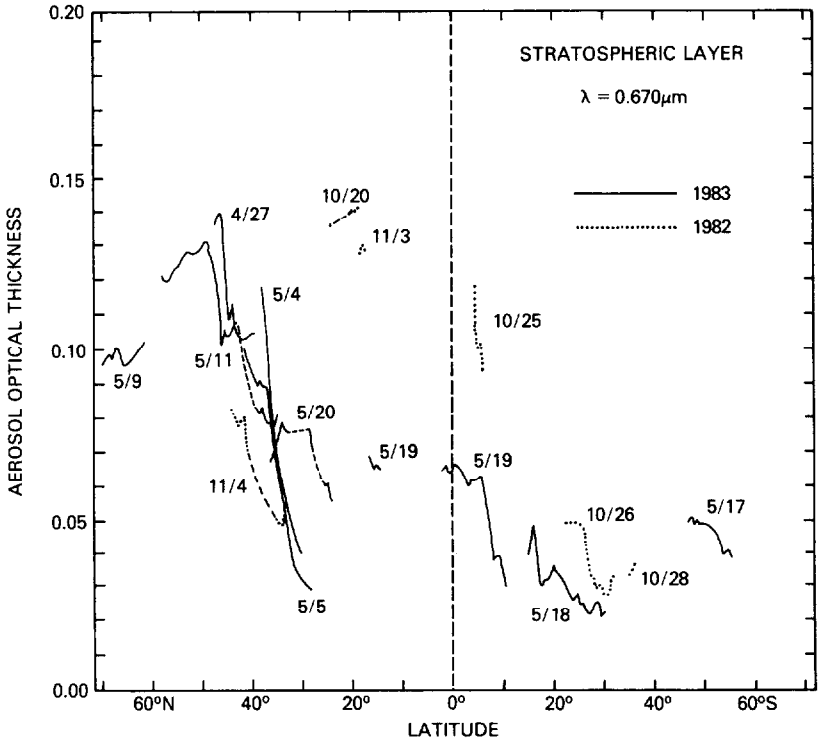

Fig. 2. Stratospheric aerosol optical thickness at 0.670 μm as a function of latitude for all measurements collected during 1982 and 1983. The dashed lines denote interpolation between observations obtained on a single day.

largest meridional gradient in optical thickness was observed on May 4 and 5, when the aircraft flights crossed a frontal region.

In addition to the gross changes in the aerosol optical thickness with space and time, the spectral dependence of the stratospheric optical thickness varies as a result of changes in the size distribution and composition of the aerosol particles. Spectral optical thickness results from the May 1983 flight are shown in Figure 3 for the wavelengths of the visible solar radiometer. The spectral optical thickness results for the October 1982 latitudinal survey are illustrated in the work of *Spinhirne* [1983]. As in Figure 2, the optical thickness results presented in Figure 3 are the average of measurements obtained over 0.5-deg intervals of latitude and are typically

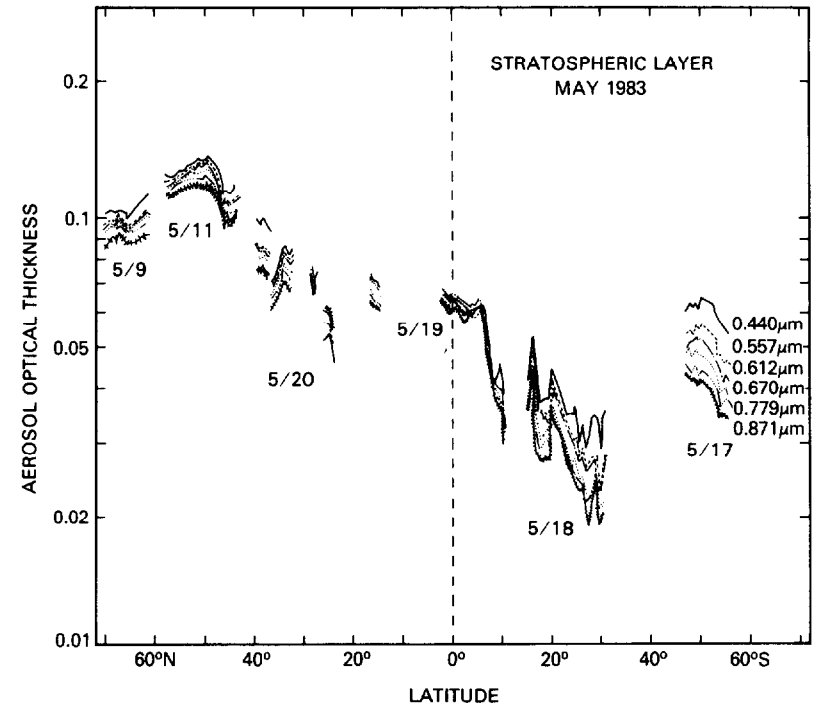

Fig. 3. Stratospheric aerosol optical thickness as a function of latitude for May 1983 and for all wavelengths in the range 0.440 μm $\leq \lambda \leq$ 0.871 μm. Only results for flights through the central Pacific are shown.

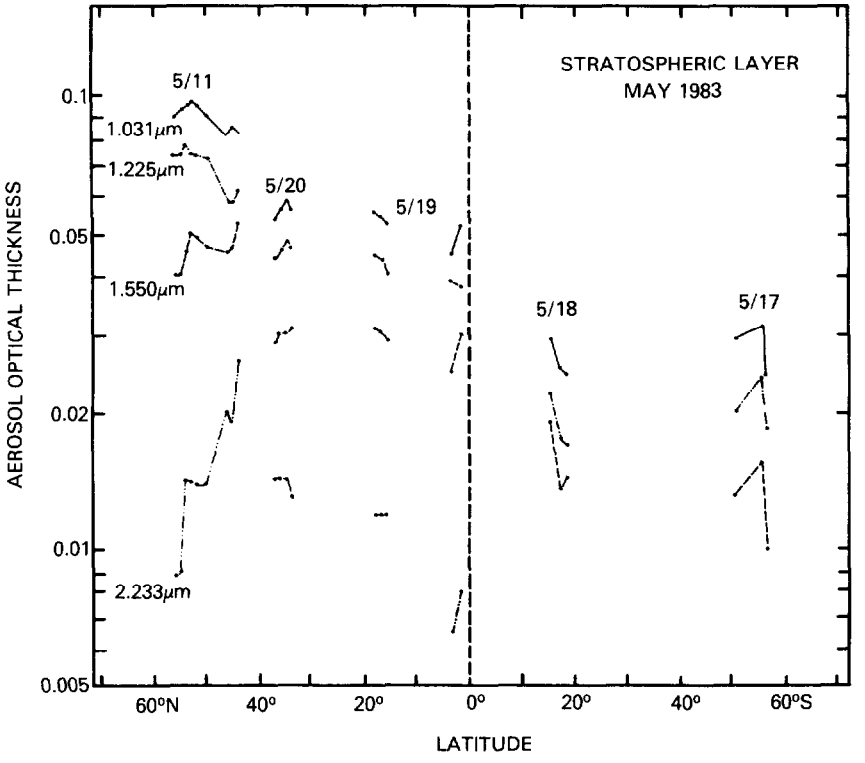

Fig. 4. Stratospheric aerosol optical thickness as a function of latitude for May 1983 and for all wavelengths in the range $1.031\ \mu m \leq \lambda \leq 2.233\ \mu m$.

derived from 10 independent observations. In order to avoid confusion from overlapping longitudes, only results for flights through the central Pacific between May 9 and May 20 are shown. The latitudinal gaps in the optical thickness measurements for an individual flight, such as those for May 20, are principally the result of overlying cirrus clouds. The interference of cirrus clouds could easily be detected from the rapid fluctuations in the measurements, though cirrus clouds could also be confirmed from the simultaneous lidar measurements.

When the spectral optical thickness is shown on a logarithmic scale, as in Figure 3, the vertical separation between wavelengths is proportional to the ratio of optical thicknesses at different wavelengths. The smallest spectral dependence of aerosol optical thickness was observed for latitudes between 5°S and 30°N. At more northerly and southerly latitudes there is an enhanced slope in the spectral dependence of optical thickness. The largest decrease of optical thickness with increasing wavelength was observed at southern hemisphere high latitudes. The large slope of spectral optical thickness in the southern hemisphere was also found in the October 1982 flight mission [cf. *Spinhirne*, 1983]. The initial inference from these results is a decrease in the number of larger particles in the aerosol size distribution for the high latitudes of the southern hemisphere relative to the size distribution in the northern tropics and subtropics.

The optical thickness results for the near-infrared wavelengths are illustrated in Figure 4 for the May 1983 flights through the central Pacific. Since these measurements were obtained with a different instrument than the visible measurements and required manual operation, the sampling interval of the observations was less frequent than that for the visible measurements. This is reflected by the coarser interval of data points in Figure 4, which are averages of approximately four observations each. Infrared observations could not be obtained on the May 9 flight owing to operational considerations.

The relative difference in the magnitude of the aerosol optical thickness over the 1.031- to 2.233-μm region is larger than that over the wavelength range of the visible measurements. The larger wavelength dependence at the longer wavelengths results from the fact that the particle concentration falls rapidly with increasing particle radius (see section 5). At the longest measurement wavelength of 2.233 μm, the optical thickness value derived from the measurements was in some regions too small to be reliably determined. The minimum value of optical thickness which could be obtained with a useful degree of accuracy from the experimental measurements was approximately 0.005, and results below this value are not presented.

The smallest stratospheric aerosol optical thicknesses in the near infrared occurred in the southern hemisphere. In addition, the largest slope in the wavelength dependence of optical thickness was in the southern hemisphere, as it was for the visible measurements. In the northern hemisphere north of 42°N, the slope of the spectral dependence of optical thickness also increases markedly. The behavior of the near-infrared optical thickness north of 42°N is a surprising result of these measurements in that the large decrease in the 2.233-μm optical thickness and the resulting change in the long-wavelength spectral dependence are not reflected at shorter wavelengths.

The uncertainties in the aerosol optical thickness measurements have been estimated using (3) and are indicated in Figures 5 through 8 (discussed in section 5.1). Typical error magnitudes are 0.002 for measurements with the largest air mass values ($m(\theta_0) \sim 5.6$), and 0.012 for measurements with the smallest air mass values ($m(\theta_0) \sim 1.5$). Measurement errors which arise from incorrect calibration values or other instrument factors would systematically bias the results. As has been mentioned previously, preflight and postflight determinations

of the instrument calibration coefficients were made. In addition, the visible solar radiometer measurements were validated against results obtained from similar instruments in operation by other research groups. In the case of the near-infrared solar radiometer, however, the uniqueness of the measurements did not permit such an intercomparison.

The validity of the near-infrared measurements can be discussed from the standprint of self-consistency as well as consistency with the visible measurements. In some instances the flights were conducted so that a large range of air mass values was experienced over a small range of latitudes on a single day. For example, the measurements on May 20 between 34°N and 40°N had air mass values that varied from approximately 3.5 to 6.0, and yet there was only a small change in the measured optical thickness at visible wavelengths. The small variation in the near-infrared optical thickness in the same region is consistent with the visible result. In addition, the spectral dependence of the near-infrared optical thickness at 42°N on May 11, where the air mass was 2.1, is consistent with the May 20 measurement at the same latitude, where the air mass was 6.0 (Figure 4). The unusual decrease in the 2.233-μm optical thickness from 42°N to 57°N was observed with the air mass increasing to 6.0 at 57°N. As is suggested by (3), an increase in air mass reduces the absolute error which would result from an incorrect calibration value. Thus it would be difficult to ascribe the 2.233-μm optical thickness variation between 42°N and 58°N to a bias in the instrument calibration.

4. Determination of Aerosol Size Distribution

Treating the stratospheric aerosol particles as a polydisperse collection of spherical particles with a single refractive index m, the integral equation relating the aerosol optical thickness to an aerosol size distribution is given by

$$\tau_a(\lambda) = \int_0^\infty \pi r^2 Q_{\text{ext}}(r, \lambda, m) n_c(r)\, dr \tag{4}$$

In this expression, r is the particle radius, $Q_{\text{ext}}(r, \lambda, m)$ is the extinction efficiency factor, and $n_c(r)$ is the unknown columnar aerosol size distribution, that is, the number of particles per unit area per unit radius interval in a vertical column through the atmosphere.

In order to determine $n_c(r)$ from spectral measurements of $\tau_a(\lambda)$, it is necessary to rewrite (4) in quadraturized form. If we measure $\tau_a(\lambda)$ at p discrete wavelengths λ and wish to infer $n_c(r)$ at q discrete radii r, a system of linear equations results which may be written in the form

$$\mathbf{g} = \mathbf{A}\mathbf{f} + \boldsymbol{\varepsilon} \tag{5}$$

where [*King*, 1982]

$$\begin{aligned} g_i &= \tau_a(\lambda_i) \qquad i = 1, 2, \cdots, p \\ A_{ij} &= \int_{r_j}^{r_{j+1}} \pi r^2 Q_{\text{ext}}(r, \lambda_i, m) h(r)\, dr \qquad j = 1, 2, \cdots, q \\ f_j &= f(r_j \le r \le r_{j+1}) \end{aligned} \tag{6}$$

The unknown error vector $\boldsymbol{\varepsilon}$ contains elements ε_i which represent the deviation between measurement (g_i) and theory ($\Sigma_j A_{ij} f_j$). This deviation arises from measurement and quadrature errors, as well as from uncertainties as to the exact form of the kernel function (in this case, $\pi r^2 Q_{\text{ext}}(r, \lambda, m)$).

In going from (4) to (6) the limits of integration have been made finite with $r_1 = r_a$ and $r_{q+1} = r_b$. Furthermore, we have made the substitution $n_c(r) = h(r) f(r)$, permitting an estimate of the size distribution, $h(r)$, to be included in the kernel matrix **A**. In this way the solution vector **f** represents the perturbation to the initially assumed size distribution required to yield a better agreement between the spectral optical thickness measurements and the regression fit to the data using the updated size distribution. This inversion process is repeated for eight iterations or until the regression fit to the optical thickness measurements reproduces the data to within the average uncertainties in the measurements [*King*, 1982].

The solution vector **f** is obtained for each iteration by using the constrained linear inversion method. For the spectral attentuation problem considered here, where standard deviation estimates $\sigma_{\tau_a}(\lambda)$ exist for all wavelengths, the solution vector **f** and solution covariance matrix **S** are given by

$$\mathbf{f} = (\mathbf{A}^T \mathbf{S}_\varepsilon^{-1} \mathbf{A} + \gamma \mathbf{H})^{-1} \mathbf{A}^T \mathbf{S}_\varepsilon^{-1} \mathbf{g} \tag{7}$$

$$\mathbf{S} = (\mathbf{A}^T \mathbf{S}_\varepsilon^{-1} \mathbf{A} + \gamma \mathbf{H})^{-1} \tag{8}$$

where $\mathbf{S}_\varepsilon$ is the measurement covariance matrix, γ is a nonnegative Lagrange multiplier, and **H** is the second derivative smoothing matrix defined by *Twomey* [1963]. If we assume that the measurement errors are uncorrelated, the measurement covariance matrix becomes diagonal with elements given by $S_{\varepsilon_{ij}} = \sigma_{\tau_a}{}^2(\lambda_i)\, \delta_{ij}$, where δ_{ij} is the Kronecker delta function. The solution standard deviations presented in the following section were obtained from the square root of the diagonal elements of the solution covariance matrix **S**, $\sigma_{n_c(r_i)} = h(r_i) S_{ii}{}^{1/2}$. The derivations of (7) and (8), together with the criteria used in selecting the Lagrange multiplier, are described in detail by *King* [1982].

5. Aerosol Size Distribution Results

The method for determining the columnar aerosol size distribution described in the preceding section has been carried out for selected data sets collected during both latitudinal surveys described in section 3. All inversions have been performed assuming that the complex refractive index of the aerosol particles is wavelength and size independent and given by $m = 1.45 - 0.00i$. Since the long-lived sulfate aerosols in the stratosphere are primarily spherical liquid droplets having a nominal 75% concentration by weight of sulfuric acid [*Hofmann and Rosen*, 1983*a*], the refractive index depends somewhat on wavelength. From the refractive indices tabulated by *Palmer and Williams* [1975] for a 75% (by weight) H_2SO_4 aqueous solution, the refractive index varies from about 1.433 at $\lambda = 0.440$ μm to $1.369 - 1.71 \times 10^{-3} i$ at $\lambda = 2.233$ μm. However, since the inverted size distribution is known to maintain its shape under various values of the real part of the refractive index and to be quite insensitive to the imaginary part of the refractive index [*King et al.*, 1978], it follows that the inversion results presented below are not significantly affected by this small degree of dispersion.

5.1. *Results for May 1983*

Optical depth measurements made at either 9 or 10 different wavelengths ranging between 0.440 and 2.233 μm have been used in the size distribution determinations for the May 1983 latitudinal survey. Owing to both the extinction cross sections (which increase significantly with radius) and the number densities (which normally decrease with radius) of the aerosol particles, the spectral range of the measurements limits the

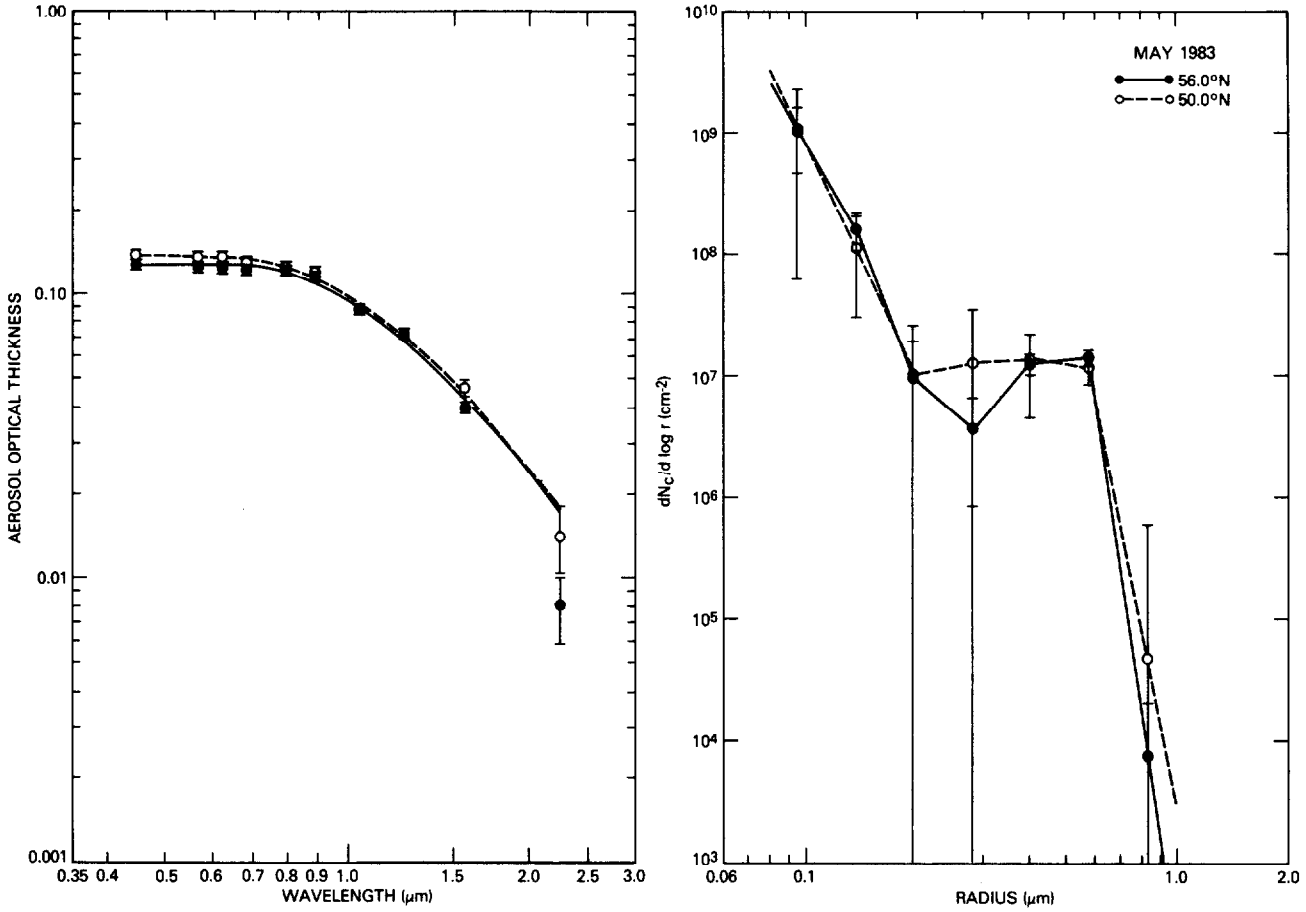

Fig. 5. Observed stratospheric aerosol optical depths and estimated size distributions for data collected during May 1983 at latitudes of 56°N and 50°N. The smooth curves on the left indicate the regression fit to the data using the inverted size distributions. Standard deviations in the optical thickness measurements are shown on the left, with estimated standard deviations in the inverted size distributions shown on the right.

radius range of maximum sensitivity ($r_a \leq r \leq r_b$). In our inversion procedure we compare the final inversion solution for three distinctly different initial estimates for the size distribution (Junge distributions with different slopes) and for various combinations of r_a in the range 0.08 μm $\leq r_a \leq$ 0.20 μm and r_b in the range 1.0 μm $\leq r_b \leq$ 4.0 μm. Of particular surprise in our analysis of these measurements was the finding that although data are available out to 2.233 μm for most latitudes, the most satisfactory inversions for all El Chichon data were obtained for r_b = 1.0 μm.

Figure 5 illustrates the aerosol optical thickness measurements and estimated size distributions for May 1983 at latitudes of 56°N and 50°N. The observed optical depths and corresponding standard deviations are shown in the left portion of the figure, while the size distributions and corresponding standard deviations obtained by inverting these data are shown in the right portion. In lieu of $n_c(r)$ or, equivalently, dN_c/dr, our size distribution results are presented in terms of dN_c/d log r, representing the number of particles per unit area per unit log radius interval in a vertical column through the atmosphere. The solid and dashed curves in the left portion of the figure indicate how the inverted size distributions reproduce the $\tau_a(\lambda)$ measurements (i.e., the direct problem $\mathbf{g} = \mathbf{Af}$).

In both data sets presented here, the spectral optical thickness measurements in the visible portion of the spectrum exhibit little spectral variation and modest negative curvature. This information alone suggests a monomodal size distribution centered around 0.35 μm, as in the July 1982 Mauna Loa optical thickness measurements of the El Chichon aerosol layer [*DeLuisi et al.*, 1983] inverted and discussed by *King et al.* [1984]. The addition of the near-infrared optical thickness measurements adds an additional constraint on the inversion solution for particles near 1.0 μm in radius (see section 5.2). This additional information, available for the first time in this experiment, results in an improved definition of the 0.35-μm mode in the size distribution as well as the definition of a second, smaller, mode in the size distribution. The regression fit to the data using these distributions is within the measurement uncertainties for most wavelengths, with the largest regression error occuring at 56°N when λ = 2.233 μm. In this case the regression error amounts to about $3\sigma_{\tau_a}$ (2.233 μm).

The aerosol size distributions illustrated in Figure 5 are well described by a bimodal modified gamma distribution of the form

$$\frac{dN_c}{d \log r} = \sum_{l=1}^{2} C_l r^{\alpha_l + 1} \exp(-b_l r) \tag{9}$$

where the mode radius for the lth mode is given by $r_{0_l} = (\alpha_l + 1)/b_l$. The distributions presented in Figure 5 were fit to (9) using the gradient expansion method from nonlinear least squares theory [*Bevington*, 1969, pp. 232–242]. The cofficients yielding the best fit to these distributions over the radius range of the inversions are presented in Table 2, where the radii limits r_a and r_b are given in Table 3.

For the mid-latitudes, where the optical thickness at 2.233 μm is greater than at the high northern latitudes, the spectral

TABLE 2. Coefficients of Bimodal (Monomodal) Modified Gamma Distribution Which Yields the Best Fit to the Inverted Size Distributions for May 1983

Date	Latitude	C_1, $cm^{-2}\ \mu m^{-(\alpha_1+1)}$	α_1	b_1, μm^{-1}	C_2, $cm^{-2}\ \mu m^{-(\alpha_2+1)}$	α_2	b_2, μm^{-1}
May 11, 1983	56.0°N	7.210×10^{12}	0.51	56.4	1.862×10^{28}	25.00	61.3
May 11, 1983	50.0°N	1.009×10^{13}	0.46	61.4	1.845×10^{17}	10.39	31.8
May 11, 1983	45.0°N	4.692×10^{13}	1.46	66.3	9.860×10^{9}	1.85	10.0
May 20, 1983	36.0°N	3.432×10^{13}	1.69	66.1	2.238×10^{9}	1.26	8.7
May 19, 1983	17.0°N	1.486×10^{12}	0.55	58.5	4.007×10^{9}	1.65	9.4
May 19, 1983	2.0°N	2.272×10^{12}	0.61	59.0	1.546×10^{14}	7.78	21.4
May 18, 1983	18.0°S	7.302×10^{5}	−2.97	0.8			
May 17, 1983	50.0°S	2.509×10^{7}	−1.85	5.5			
May 17, 1983	55.5°S	5.352×10^{6}	−2.48	3.8			

optical thickness exhibits negative curvature throughout the wavelength range 0.440 $\mu m \le \lambda \le 2.233$ μm. Figure 6 illustrates the spectral optical depth measurements and corresponding size distributions for three latitudes between 45°N and 17°N. With the single exception of the optical thickness measurement at $\lambda = 1.225$ μm (45°N), the inverted size distributions reproduce the measurements to within the measurement uncertainties. Owing in part to the small standard deviations in the measurements and in part to the good regression fit to the data, the estimated uncertainties in the size distributions are small throughout the radius range 0.08 $\mu m \le r \le 1.0$ μm. The resulting bimodal size distributions were fit to (9), and the optimum coefficients were derived for each distribution. These results are presented in Table 2.

In the tropical latitudes between 2°N and 18°S, illustrated in Figure 7, measurements were available for nine wavelengths between 0.440 and 1.550 μm. At these latitudes the uncertainties in the measured optical depths are noticeably larger than in any of the previous cases. This is a result of both the smaller aerosol optical depths and the fact that the observations were obtained at a smaller air mass than at the higher latitudes of the northern hemisphere. These two factors contribute to greater uncertainties in the derived size distributions. The strong negative curvature in the 2°N data leads to a bimodal size distribution similar to the bimodal distributions obtained at higher latitudes of the northern hemisphere. Owing to the lack of a measurement at 2.233 μm, coupled with larger measurement uncertainties, the first mode in the size distribution is determined with a large uncertainty. This bimodal size distribution was again fit to (9), with the resulting bimodal coefficients presented in Table 2.

At all latitudes of the southern hemisphere, the optical thickness monotonically decreases throughout the wavelength range of the measurements, with the suggestion that the peak aerosol optical thickness is at some ultraviolet wavelength of less than 0.440 μm. The spectral optical depths and corresponding size distributions are illustrated for 18°S in Figure 7 and for 50°S and 55.5°S in Figure 8. These size distributions were all fit to the first mode of the modified gamma distribution ($l = 1$) given by (9), with the resulting monomodal size distribution parameters presented in Table 2.

In addition to determining coefficients of a monomodal or bimodal size distribution, a number of additional parameters have been derived from the size distribution results. These parameters, presented in Table 3, include the effective radius

$$r_{\text{eff}} = \int_{r_a}^{r_b} r^3 n_c(r)\, dr \Big/ \int_{r_a}^{r_b} r^2 n_c(r)\, dr$$

columnar mass loading M_c, ratio of the aerosol volume extinction coefficient to volume backscattering coefficient S in units of steradians, and aerosol asymmetry factor g. The S ratio and asymmetry factor have been determined at the ruby lidar wavelength ($\lambda = 0.6943$ μm) where spherical droplets having a 75% concentration by weight of sulfuric acid have a particle density of 1.65 g cm^{-3} and a refractive index of $m = 1.428 - 2.07 \times 10^{-8} i$ [*Palmer and Williams*, 1975].

5.2. *Effects of Wavelength Range*

Since the optical depths obtained during May 1983 include results from both the visible and near-infrared solar radiometers, whereas the October and November 1982 aircraft data include measurements from only the visible solar radiometer, it is important to examine the effect of wavelength range on the inverted size distribution results.

Figure 9 compares two different size distributions obtained by inverting the May 1983 measurements at 36°N. The first distribution is the one obtained by inverting data from the full wavelength range 0.440 $\mu m \le \lambda \le 2.233$ μm and is the same result as that presented in Figure 6. The second distribution is obtained by using data from the visible solar radiometer only (0.440 $\mu m \le \lambda \le 0.871$ μm). The magnitudes of the solution uncertainties presented in Figures 6 and 9 suggest that the presence of observations in the near-infrared improves the inversion results at the small-particle end of the distribution. In the absence of any directly observed size distributions with which to draw definitive conclusions, we offer the following plausible arguments to help explain these results.

TABLE 3. Radius Range, Effective Radius, Columnar Mass Loading, and Extinction to Backscatter Ratio S and Asymmetry Factor g at 0.6943 μm for Inverted Size Distributions Obtained During October and November 1982 and May 1983

						$\lambda = 0.6943$ μm	
Date	Latitude	r_a, μm	r_b, μm	r_{eff}, μm	M_c, mg m^{-2}	S, sr	g
Nov. 4, 1982	44.0°N	0.15	1.0	0.50	29	55	0.749
Nov. 4, 1982	44.0°N	0.10	1.0	0.37	16	63	0.739
Oct. 20, 1982	24.5°N	0.10	1.0	0.44	47	56	0.739
Nov. 3, 1982	17.8°N	0.10	1.0	0.43	43	58	0.745
Oct. 25, 1982	5.0°S	0.10	1.0	0.39	43	48	0.709
Oct. 26, 1982	24.0°S	0.10	1.0	0.28	17	57	0.703
Oct. 26, 1982	32.0°S	0.10	1.0	0.26	11	63	0.700
Oct. 28, 1982	35.0°S	0.10	1.0	0.22	13	55	0.665
May 11, 1983	56.0°N	0.08	1.0	0.21	42	51	0.731
May 11, 1983	50.0°N	0.08	1.0	0.21	45	53	0.730
May 11, 1983	45.0°N	0.08	1.0	0.34	38	53	0.736
May 20, 1983	36.0°N	0.08	1.0	0.38	26	54	0.739
May 19, 1983	17.0°N	0.08	1.0	0.36	25	53	0.737
May 19, 1983	2.0°N	0.10	1.0	0.40	22	56	0.753
May 18, 1983	18.0°S	0.15	1.0	0.41	12	56	0.727
May 17, 1983	50.0°S	0.15	1.0	0.33	16	67	0.729
May 17, 1983	55.5°S	0.15	1.0	0.34	13	66	0.726

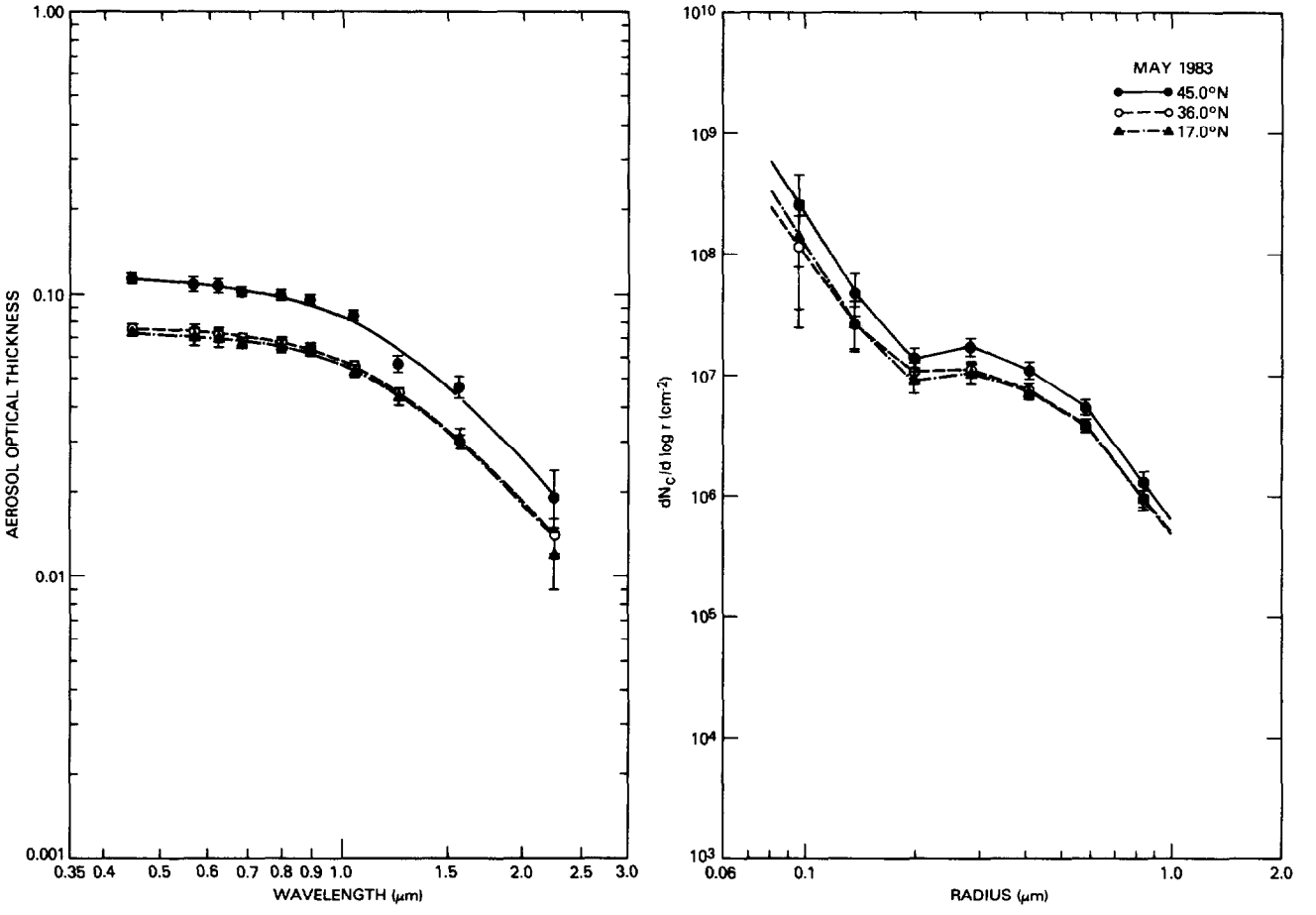

Fig. 6. As in Figure 5 except for data collected at 45°N, 36°N, and 17°N.

With data available only from 0.440 to 0.871 μm, sufficient latitude exists in the size distribution at a radius of 1.0 μm that it is fairly easy to obtain a size distribution which is capable of reproducing the measurements. This size distribution, however, would also be capable of predicting the optical thickness in the near infrared where no measurements are available. This extrapolation is naturally less reliable the further it is extended from the wavelength interval used in deriving the size distribution. When data are available in the near infrared, as they were during May 1983, the additional data pose a tight constraint on the particle distribution at 1.0 μm.

At 36°N, as well as at 56°N, these additional data pose a tight constraint on the number of large particles present in the distribution. As a consequence, the large-particle end of the distribution is obtained with greater confidence. In order to reproduce the optical thickness measurements at the short-wavelength end of the spectrum, the small-particle end of the size distribution must change, since the large-particle end of the distribution is well defined. In Figure 9 the large uncertainties in the small-particle end of the size distribution are those associated with data from the visible solar radiometer, whereas the small uncertainties are associated with results obtained using the full wavelength range available.

In the southern hemisphere, where the spectral optical depths in the visible wavelength region have a much larger spectral variation, the effect of restricting the wavelength range is quite different. Figure 10 illustrates the inverted size distributions obtained at 55.5°S using the restricted wavelength range (0.440 μm $\leq \lambda \leq$ 0.871 μm) and the full wavelength range (0.440 μm $\leq \lambda \leq$ 1.550 μm). Comparing Figure 10 with the optical thickness measurements presented in Figure 8, it is readily apparent that the restricted wavelength range is characterized by optical thicknesses which exhibit a modest positive curvature. This is necessarily manifested in the inverted size distribution (Figure 10). When the full data set is examined, however, it appears as if τ_a(0.871 μm) is systematically high, reflecting a possible measurement error. When data over the entire wavelength range are used, the inverted size distribution has a negative curvature in order to account for the reduced optical depths in the near infrared. These examples help to emphasize the obvious, that the inverted size distribution is only as good as the input measurements used to derive it and that a greater spectral range for the measurements minimizes the influence of any single observation.

5.3. *Results for October and November 1982*

Figure 11 illustrates the size distributions obtained by inverting spectral optical thickness measurements obtained during October and November 1982 from 44°N to 35°S. The spectral optical depths and estimated standard deviations are tabulated and illustrated by *Spinhirne* [1983]. Bearing in mind the limitations in the October and November results and the fact that data are available only for six wavelengths between 0.440 and 0.871 μm, one sees that the northern latitudes are characterized by broad monomodal size distributions and the southern latitudes are characterized by distributions whose shapes are more typical of background nonvolcanic conditions (see, for example, *King et al.* [1984]).

The closest observations with which to compare our fall 1982 results are those obtained by *Hofmann and Rosen* [1983*a*] using balloon-borne particle counters. These results, obtained at Del Rio, Texas (29.2°N) on October 23, 1982, have

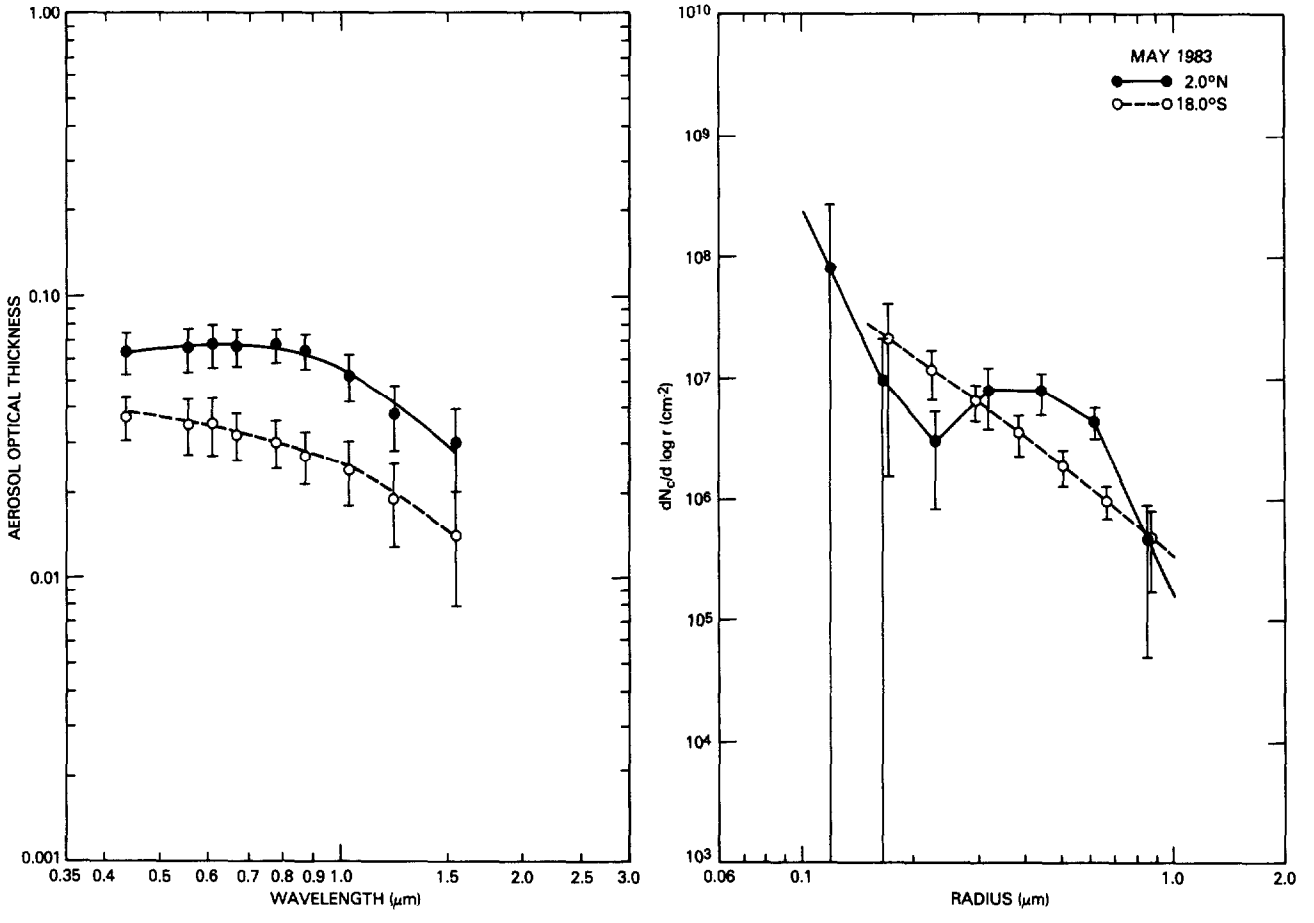

Fig. 7. As in Figure 5 except for data collected at 2°N and 18°S.

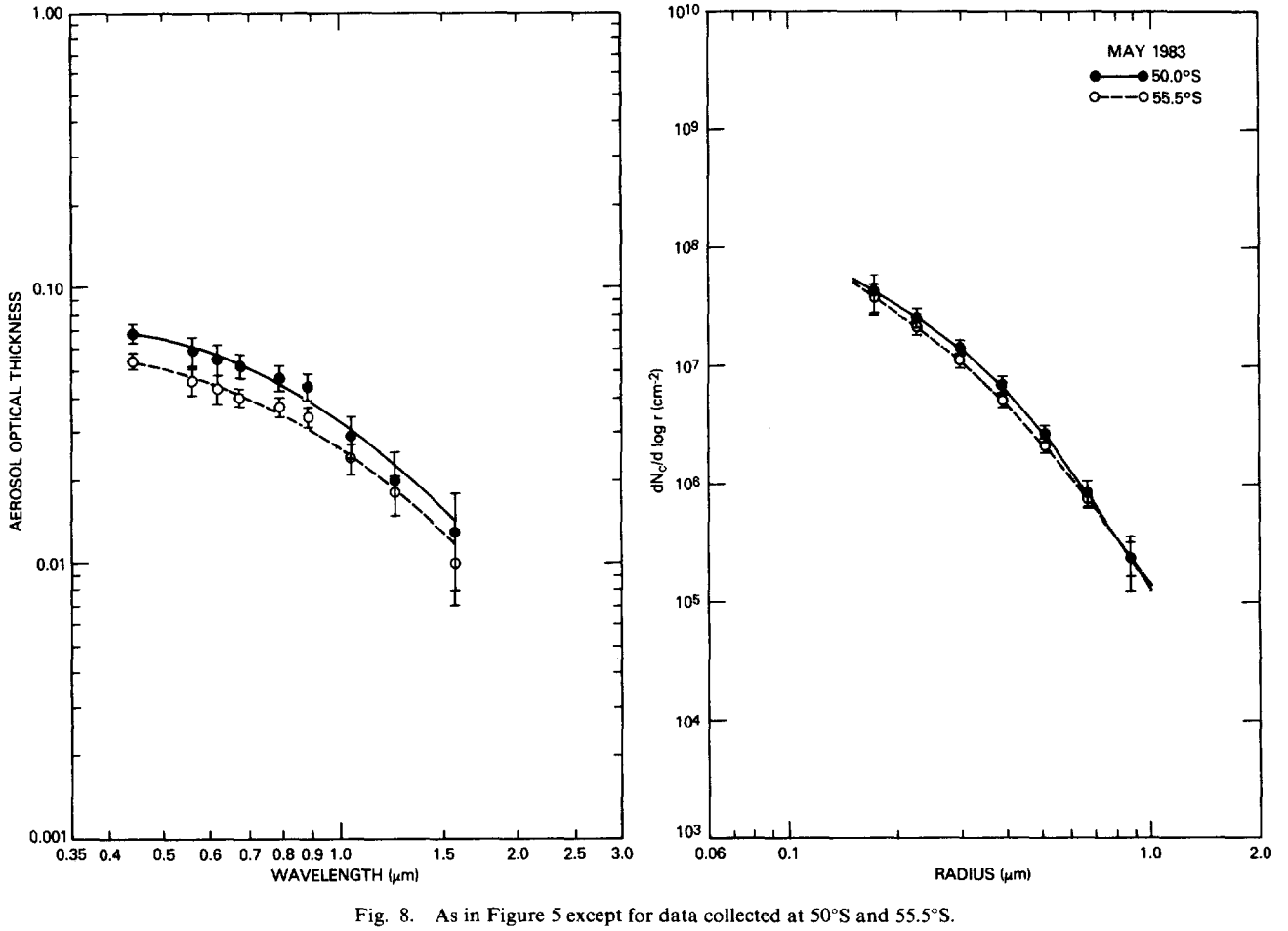

Fig. 8. As in Figure 5 except for data collected at 50°S and 55.5°S.

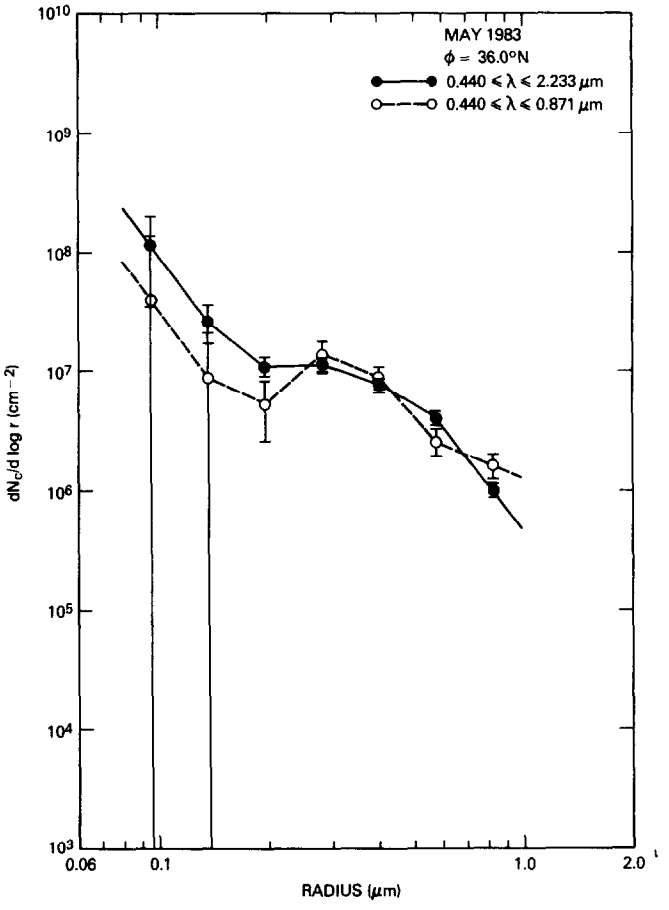

Fig. 9. Comparison of size distributions and estimated standard deviations obtained by inverting solar radiometer data collected over two different wavelength intervals during May 1983 at 36°N. In one case the data used in the inversion are restricted to the wavelength interval 0.440 μm $\leq \lambda \leq$ 0.871 μm, and in the other case data are used from the full wavelength range available.

been integrated over the altitude range from 21.5 to 24.5 km and modeled as a bimodal lognormal size distribution [*Hofmann and Rosen*, 1983*b*]. *King et al.* [1984] scaled these results to the optical thickness at 0.55 μm, from which we find that our results for 17.8°N compare favorably with the principal mode in *Hofmann and Rosen*'s [1983*b*] distribution. In addition to the principal mode at 0.27 μm, Hofmann and Rosen observed a narrow-particle mode at 1.0 μm, a result which we are insensitive to with our data.

The effective radius, columnar mass loading, extinction to backscatter ratio, and asymmetry factor for October and November 1982 are presented in Table 3. In converting monostatic ruby lidar measurements to optical thickness, *Swissler et al.* [1983] assumed that $S = 42.8$ sr for latitudes north of 26°S and 58.8 sr for latitudes south of 26°S. From Table 3 our results suggest values of 56.2 sr north of 26°S and 59.0 sr south of 26°S, respectively. The agreement in both cases is within the range allowed by errors involved in the calculations.

6. Discussion

All results presented in this paper show a consistent pattern in the latitudinal variation of the stratospheric aerosol size distribution. For the May 1983 measurements in the northern mid-latitudes, the variation in the observed spectral dependence of optical thickness is small, especially in the visible wavelength region (0.440 μm $\leq \lambda \leq$ 0.871 μm). The derived size distributions in the latitudes between 17°N and 45°N show a consistent pattern of a bimodal size distribution with a small-particle mode having a mode radius of less than 0.1 μm and a large-particle mode having a mode radius of about 0.28 μm. North of 45°N the size distribution results suggest a relative loss of particles at radii near 1.0 μm and a relative gain of particles in the small-particle mode. These results are consistent with the discussion by *Hofmann and Rosen* [1985], who propose a mechanism for evaporation and reformation of particles in the stratosphere whereby poleward transport at northern latitudes leads to stratospheric warming and the evaporation of larger particles. Subsequent transport to the south results in cooling, with a requisite formation of small particles by condensation.

The inverted size distributions at tropical latitudes are of poorer quality than those at the higher latitudes of the northern hemisphere, partly because they are based on fewer measurements and partly because the observations were obtained when the air mass was particularly small. However, the results which were obtained indicate a bimodal size distribution at 2°N, consistent with other results obtained in the northern hemisphere, and a broad monomodal distribution at 18°S, consistent with other results obtained in the southern hemisphere.

Possibly the most significant finding from the size distribution determinations was the clear distinction between the northern and southern hemisphere stratospheric aerosol size distributions. For the October 1982 measurements the size distributions throughout the low northern latitudes, where the

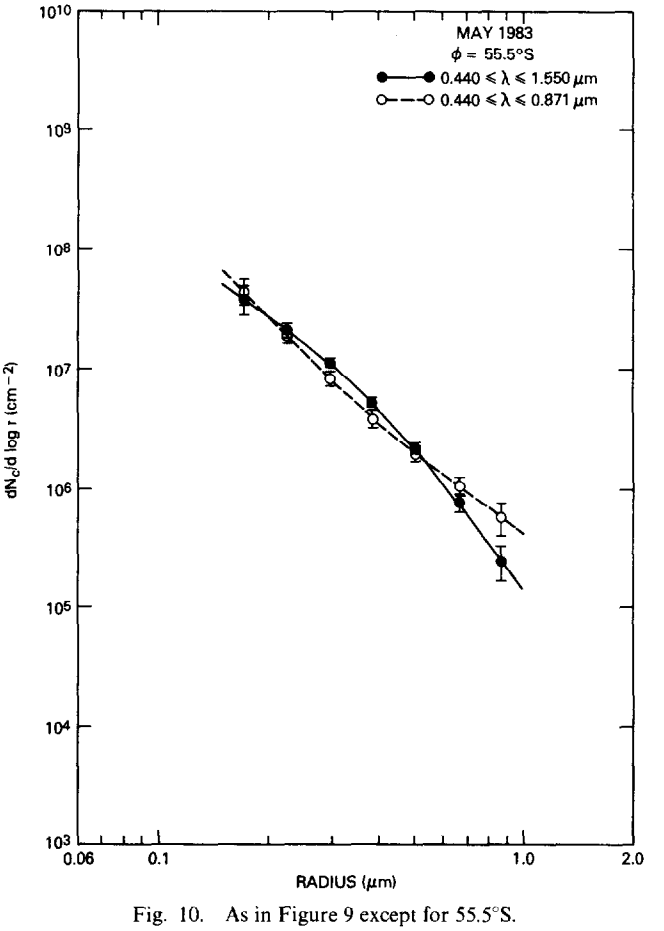

Fig. 10. As in Figure 9 except for 55.5°S.

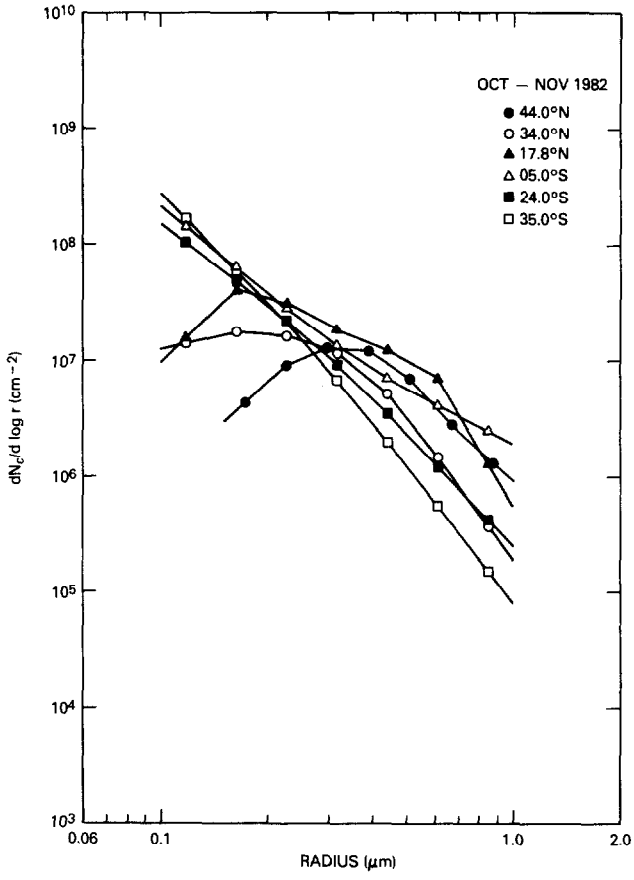

Fig. 11. Inverted size distributions for October and November 1982 for latitudes from 44°N to 35°S, where optical thickness data were only available from the visible solar radiometer (0.440 $\mu m \leq \lambda \leq 0.871$ μm).

bulk of the eruption cloud was confined, show a characteristic single mode distribution with a mode radius of about 0.25 μm. In the southern mid-latitudes, even though the elevated values of the optical thickness suggest that debris from the eruption cloud entered the southern hemisphere, the size distribution is much closer to the shape of a background stratospheric aerosol size distribution than a postvolcanic size distribution, lacking the large particle mode that characterized the main eruption cloud in the northern hemisphere. During the early phases in the development of the eruption cloud in the northern hemisphere, the aerosol layer was separated vertically into two principal layers, with the largest particle concentration confined to the upper layer [*Hofmann and Rosen*, 1983*b*]. Monostatic lidar observations [*McCormick and Swissler*, 1983] have shown that the lower stratospheric layer during October 1982 extended into the southern hemisphere and that the upper layer was largely confined to the latitude range 5°S–36°N. Also, *Pollack et al.* [1983] have stated that the aerosol transport to the southern hemisphere was confined to lower stratospheric altitudes. Our results are in apparent accord with these results. The size distribution results from the May 1983 observations show a similar differentiation between the size distributions in the northern and southern hemispheres.

7. Summary and Conclusions

In this paper, measurements have been presented of the spectral optical thickness of the El Chichon stratospheric aerosol layer obtained during an airborne latitudinal survey in late April and early May 1983. The observations include measurements at 10 discrete wavelengths from 0.440 to 2.233 μm and cover latitudes from 68°N to 56°S. Columnar aerosol size distributions of the stratosphere have been derived by inverting the aerosol optical thickness measurements as a function of wavelength. In addition, columnar aerosol size distributions have been derived from spectral aerosol optical depth measurements obtained during an earlier airborne latitudinal survey conducted during late October and early November 1982. During this experiment, previously reported by *Spinhirne* [1983], optical thickness measurements were acquired at six discrete wavelengths from 0.440 to 0.871 μm and over latitudes from 44°N to 36°S.

An evident increase in the stratospheric optical thickness from the El Chichon eruption was found at all locations where observations were obtained. In late October and early November 1982 the bulk of the increase in stratospheric optical thickness was confined to latitudes between 6°S and 30°N, where the peak optical thickness at the midvisible wavelengths was about 0.14. During late April and early May 1983 the peak optical thickness was also near 0.14, but the region of maximum optical thickness had moved to latitudes between 35°N and 55°N. In the northern tropical latitudes the optical thickness had dropped to approximately one third of its value during the previous experiment. The optical thickness in the southern hemisphere was found to be approximately one fourth of that for the northern hemisphere at the mid-visible wavelengths.

The spectral optical thickness and derived size distributions obtained from both aircraft flight missions show latitudinal regions with similar characteristics. For the October 1982 measurements the two regions were the southern hemisphere below 6°S and the major region of the cloud within low latitudes of the northern hemisphere. The size distribution in the southern hemisphere was similar in shape to that of a background stratospheric aerosol distribution. Within the northern hemisphere during October 1982, the size distribution results show the characteristic enhancement of larger particles with a single mode peaking near 0.25 μm. For May 1983 the spectral optical thickness and size distribution for the southern hemisphere were similar to the results obtained from the October 1982 observations. However, a bimodal distribution was derived for northern latitudes. North of 45°N a falloff in the relative concentration of the largest particles was found, and the smaller-particle mode was enhanced.

Airborne solar radiometer measurements have been shown to be a useful technique for studying latitudinal variations of optical and related particle size characteristics of the stratospheric aerosol layer, at least for the enhanced conditions which resulted from the El Chichon eruption. The measurements at near-infrared wavelengths, obtained for the first time as part of the May 1983 survey, have proven to be a valuable addition to the size distribution retrieval procedure. A significant improvement in the experimental technique over these inital measurements should be possible. However, it is doubtful whether solar radiometer measurements could ever be applied with sufficient accuracy to study stratospheric aerosol particles under background conditions.

Acknowledgments. The authors are grateful to Hongwoo Park for assistance with observations, Steven L. Palm and William D. Hart for assistance in processing the solar transmission measurements, and Howard G. Meyer for assistance in performing the size distribution inversions.

REFERENCES

Barth, C. A., R. W. Sanders, R. J. Thomas, G. E. Thomas, D. M. Jakosky, and R. A. West, Formation of the El Chichon aerosol cloud, *Geophys. Res. Lett.*, *10*, 993–996, 1983.

Bevington, P. R., *Data Reduction and Error Analysis for the Physical Sciences*, 336 pp., McGraw-Hill, New York, 1969.

DeLuisi, J. J., E. G. Dutton, K. L. Coulson, T. E. DeFoor, and B. G. Mendonca, On some radiative features of the El Chichon volcanic stratospheric dust cloud and a cloud of unknown origin observed at Mauna Loa, *J. Geophys. Res.*, *88*, 6769–6772, 1983.

Dutton, E. G., and J. J. DeLuisi, Spectral extinction of direct solar radiation by the El Chichon cloud during December 1982, *Geophys. Res. Lett.*, *10*, 1013–1016, 1983*a*.

Dutton, E. G., and J. J. DeLuisi, Optical thickness features of the El Chichon stratospheric debris cloud, in *Proceedings of the Fifth Conference on Atmospheric Radiation*, pp. 361–363, American Meteorological Society, Boston, Mass., 1983*b*.

Evans, W. F. J., and J. B. Kerr, Estimates of the amount of sulfur dioxide injected into the stratosphere by the explosive volcano eruptions: El Chichon, mystery volcano, Mt. St. Helens, *Geophys. Res. Lett.*, *10*, 1049–1052, 1983.

Hofmann, D. J., and J. M. Rosen, Stratospheric sulfuric acid fraction and mass estimate for the 1982 volcanic eruption of El Chichon, *Geophys. Res. Lett.*, *10*, 313–316, 1983*a*.

Hofmann, D. J., and J. M. Rosen, Sulfuric acid droplet formation and growth in the stratosphere after the 1982 eruption of El Chichon, *Science*, *222*, 325–327, 1983*b*.

Hofmann, D. J., and J. M. Rosen, Delayed production of sulfuric acid condensation nuclei in the polar stratosphere from El Chichon volcanic vapors, *J. Geophys. Res.*, *90*, 2341–2354, 1985.

King, M. D., Sensitivity of constrained linear inversions to the selection of the Lagrange multiplier, *J. Atmos. Sci.*, *39*, 1356–1369, 1982.

King, M. D., D. M. Byrne, B. M. Herman, and J. A. Reagan, Aerosol size distributions obtained by inversion of spectral optical depth measurements, *J. Atmos. Sci.*, *35*, 2153–2167, 1978.

King, M. D., Harshvardhan, and A. Arking, A model of the radiative properties of the El Chichon stratospheric aerosol layer, *J. Clim. Appl. Meteorol.*, *23*, 1121–1137, 1984.

McCormick, M. P., and T. J. Swissler, Stratospheric aerosol mass and latitudinal distribution of the El Chichon eruption cloud for October 1982, *Geophys. Res. Lett.*, *10*, 877–880, 1983.

McCormick, M. P., T. J. Swissler, W. H. Fuller, W. H. Hunt, and M. T. Osborn, Airborne and ground-based lidar measurements of the El Chichon stratospheric aerosol from 90°N to 56°S, *Geofis. Int.*, *23*, 187–221, 1984.

Oberbeck, V. R., E. F. Danielsen, K. G. Suetsinger, G. V. Ferry, W. Fong, and D. M. Hayes, Effects of the eruption of El Chichon on stratospheric aerosol size and composition, *Geophys. Res. Lett.*, *10*, 1021–1024, 1983.

Palmer, K. F., and D. Williams, Optical constants of sulfuric acid; Application to the clouds of Venus, *Appl. Opt.*, *14*, 208–219, 1975.

Pollack, J. B., and T. P. Ackerman, Possible effects of the El Chichon volcanic cloud on the radiative budget of the northern tropics, *Geophys. Res. Lett.*, *10*, 1057–1060, 1983.

Pollack, J. B., O. B. Toon, E. F. Danielson, D. J. Hofmann, and J. M. Rosen, The El Chichon volcanic cloud: An introduction, *Geophys. Res. Lett.*, *10*, 989–992, 1983.

Shaw, G. E., Error analysis of multi-wavelength sun photometry, *Pure Appl. Geophys.*, *114*, 1–14, 1976.

Shaw, G. E., Sun photometry, *Bull. Am. Meteorol. Soc.*, *64*, 4–10, 1983.

Spinhirne, J. D., El Chichon eruption cloud: Latitudinal variation of the spectral optical thickness for October 1982, *Geophys. Res. Lett.*, *10*, 881–884, 1983.

Spinhirne, J. D., M. G. Strange, and L. R. Blaine, Solar infrared photometer, *J. Oceanic Atmos. Tech.*, *2*, 264–267, 1985.

Swissler, T. J., M. P. McCormick, and J. D. Spinhirne, El Chichon eruption cloud: Comparison of lidar and optical thickness measurements for October 1982, *Geophys. Res. Lett.*, *10*, 885–888, 1983.

Thomason, L. W., B. M. Herman, R. M. Schotland, and J. A. Reagan, Extraterrestrial solar flux measurement limitations due to a Beer's law assumption and uncertainty in local time, *Appl. Opt.*, *21*, 1191–1195, 1982.

Twomey, S., On the numerical solution of Fredholm integral equations of the first kind by the inversion of the linear system produced by quadrature, *J. Assoc. Comput. Mach.*, *10*, 97–101, 1963.

Uplinger, W. G., A simple model for relative air mass, in *Proceedings of the Fourth Conference on Atmospheric Radiation*, pp. 108–110, American Meteorological Society, Boston, Mass., 1981.

M. D. King, and J. D. Spinhirne, Laboratory for Atmospheres, NASA Goddard Space Flight Center, Greenbelt, MD 20771

(Received January 5, 1985;
revised May 15, 1985;
accepted May 17, 1985.)